Atmos. Meas. Tech., 9, 5063–5075, 2016
www.atmos-meas-tech.net/9/5063/2016/
doi:10.5194/amt-9-5063-2016

Atmospheric Measurement Techniques
Open Access
EGU

Airborne laser scan data: a valuable tool with which to infer weather radar partial beam blockage in urban environments

Roberto Cremonini[1,3], **Dmitri Moisseev**[1,4], **and Venkatachalam Chandrasekar**[1,2]

[1]Department of Physics, University of Helsinki, Helsinki, Finland
[2]Colorado State University, Fort Collins, Colorado, USA
[3]ARPA Piemonte, Dipartimento Sistemi Previsionali, Turin, Italy
[4]Finnish Meteorological Institute, Helsinki, Finland

Correspondence to: Roberto Cremonini (rcremoni@mappi.helsinki.fi)

Received: 8 March 2016 – Published in Atmos. Meas. Tech. Discuss.: 18 March 2016
Revised: 15 September 2016 – Accepted: 15 September 2016 – Published: 17 October 2016

Abstract. High-spatial-resolution weather radar observations are of primary relevance for hydrological applications in urban areas. However, when weather radars are located within metropolitan areas, partial beam blockages and clutter by buildings can seriously affect the observations. Standard simulations with simple beam propagation models and digital elevation models (DEMs) are usually not able to evaluate buildings' contribution to partial beam blockages. In recent years airborne laser scanners (ALSs) have evolved to the state-of-the-art technique for topographic data acquisition. Providing small footprint diameters (10–30 cm), ALS data allow accurate reconstruction of buildings and forest canopy heights. Analyzing the three weather C-band radars located in the metropolitan area of Helsinki, Finland, the present study investigates the benefits of using ALS data for quantitative estimations of partial beam blockages. The results obtained applying beam standard propagation models are compared with stratiform 24 h rainfall accumulation to evaluate the effects of partial beam blockages due to constructions and trees. To provide a physical interpretation of the results, the detailed analysis of beam occultations is achieved by open spatial data sets and open-source geographic information systems.

1 Introduction

Rapid, uncontrolled spatial growth and densification create settlements in inappropriate areas most likely to be exposed to natural hazards. In 2014, about 54 % of the world's population lived in urban areas (United Nations, 2014), with an increase from 43 % in 1990. According to the UN Office for Disaster Risk Reduction (UNISDR, 2011), over 80 % of disasters reported by national sources occurred in urban areas. Moreover, in 2014, nearly 56 % of cities, representing 62 % of city inhabitants worldwide, were at high risk of exposure to at least one type of natural disaster. As reported in the CRED/OFDA International Disaster Database (Guha-Sapir et al., 2016), hydro-meteorological hazards (floods, cyclones and storms) are the most prevalent types. Einfalt et al. (2004) reported several applications of weather radar rainfall to urban hydrology demonstrating widespread increasing of weather radar observations in urban environment. However, recent studies have demonstrated that up to 100 m resolution quantitative precipitation estimations (QPEs) and 1 min scans are required in order to be useful for pluvial flood forecast in urban environment (Berne et al., 2004; Ten Veldhuis et al., 2014). As the spatial resolution of weather radar observations decreases with the distance from the antenna, the sensor cannot be placed too far from the target area for urban hydrology. However, when the weather radar is located within urbanized areas, buildings, masts and trees produce several partial beam blockages (PBBs) and large return clutter. Beam occultations lead to underestimation of precipitation rate, especially during wintertime when the upper part of the radar volume is filled with snow and ice crystals. Therefore, the identification of areas where the radar-based QPE is affected by PBBs is mandatory for successful hydrological applications in urbanized areas. Several beam blockage correction schemes can be applied in order to minimize the

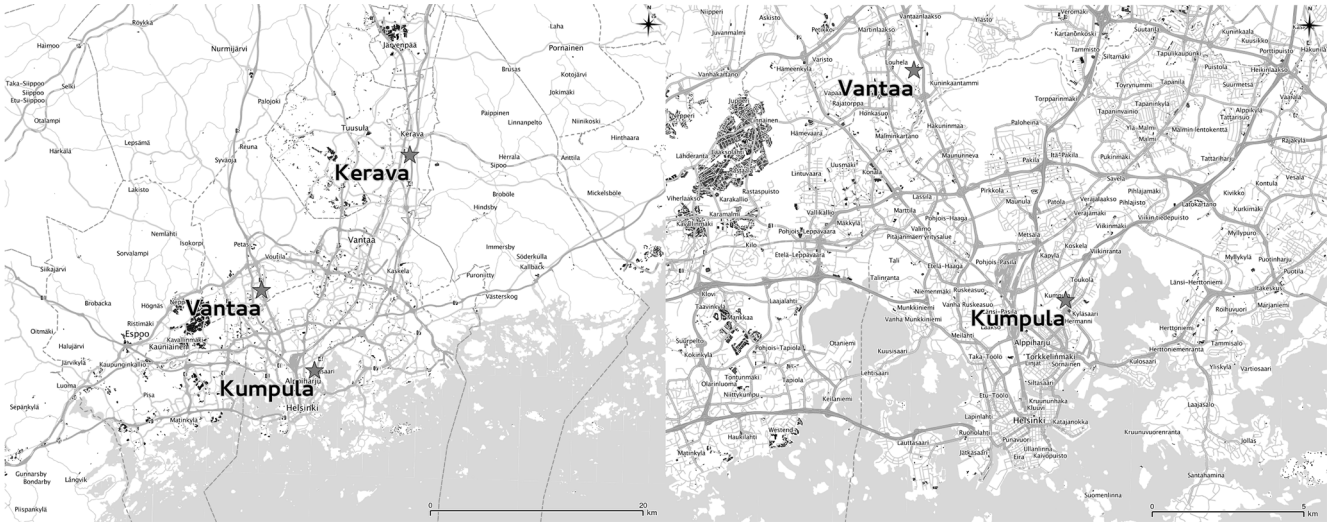

Figure 1. The weather radar locations within the metropolitan area of Helsinki, Finland. Left: the map overview of the three radar sites. Right: the detailed map for Vantaa and Kumpula radar indicating main roads, railways and buildings.

effect of PBBs on QPEs (Kitchen et al., 1994; Fulton et al., 1998; Bech et al., 1968). The development of polarimetry has also demonstrated that QPEs based on the specific propagation phase (KDP) are relatively insensible to partial beam blockages (Giangrande and Ryzhkov, 2005; Lang et al., 2009). However, PBB-correction schemes based on KDP cannot be applied when radar observations are in snow or ice (Zhang et al., 2013); moreover, many operational weather radar are still in single polarization. As demonstrated in several studies (Kucera et al., 2004; Fornasiero et al., 2006; Krajewski et al., 2006), accurate radar visibility maps can be obtained by applying beam standard atmospheric propagation models (Doviak and Zrnić, 1984) coupled with high-resolution digital elevation models (DEMs). Furthermore, Krajewski et al. (2006) also demonstrated that PBBs can be successfully estimated by modeling radar visibility using accurate DEM data and a geographic information system (GIS). Unfortunately, buildings, infrastructure (masts, power lines) and forest canopy are not represented in DEMs by definition; therefore, the estimated radar visibility in urban areas tends to be optimistic, missing heavy beam blockages due to obstacles close to the radar antenna. In the recent years lidar (light detection and ranging or laser-induced direction and ranging) technology has proven to be the most promising data source to fill the gap between DEMs and actual surfaces. Recently, airborne laser scanning (ALS) data, the state-of-the-art technique for topographic data acquisition, have provided small footprint diameters (10–30 cm), allowing accurate estimations of buildings, constructions and forest canopy heights (Shan et al., 2008). In this paper the C-band weather radar network PBBs in Helsinki, Finland, are evaluated. For the first time, this study investigates the benefits of using ALS data in the metropolitan area with respect to DEMs for quantitative estimations of radar beam occultations. Moreover, this study deals with uncertainties related to PBB estimations: focusing on more relevant obstacles, the proposed approach evaluates uncertainties due to antenna pointing imprecision. Finally, the physical interpretation of the results is obtained by analyzing the results by open data, provided by the Finnish publishing platform AAVA (http://avaa.tdata.fi/web/avaa/tietoa-palvelusta), and open-source GIS tools. Section 2 outlines the radar data, ALS data set and methodology. The discussion of results and conclusions are presented respectively in Sects. 3 and 4.

2 Data and methodology

Laser scanning or lidar offers the most accurate method for collecting elevation data for the production of digital elevation or surface models. Airborne laser scanning is a rapid, highly accurate and efficient method of capturing 3-D data of large areas, such as agricultural or forestry sites, urban areas or industrial plants; its development goes back to the 1970s and 1980s, with an early NASA system and other attempts in the USA and Canada (Ackermann et al., 1999). The benefits of ALS data consist of significantly improved accuracy, lower processing costs and higher automation; thus, performing national laser scanning is already completed or planned in many countries. For example, in Germany large parts of the country have been scanned and the work is conducted on a federal basis. In 2008 the National Land Survey of Finland (NLS) began collecting airborne laser scanning data throughout Finland to provide a new high-detailed terrain elevation model. The Finnish ALS data are organized in 3 km by 3 km tiles with an average point density of about 0.5 points m^{-2}. According to Ahokas and Kaartinen (2013), the ALS accuracy obtained in all various sur-

Table 1. Helsinki weather radar main characteristics.

Radar	Longitude	Latitude	Altitude	Beamwidth
Kumpula (KUM)	24.269° E	60.204° N	83 m	1.05°
Vantaa (VAN)	24.869° E	60.270° N	83 m	0.98°
Kerava (KER)	25.114° E	60.388° N	59 m	1.00°

face types was better than 30 cm (RMSE). ALS data are geo-located using the ETRS89 – ETRS-TM35FIN geographical coordinate system. Since 2005 the Finnish Meteorological Institute (FMI) and Vaisala Oyj have established and maintained the high-resolution mesoscale network called Helsinki Testbed (http://testbed.fmi.fi/). The aim was to develop an internationally recognized platform where scientists could deploy their measurement devices and monitor small-scale weather phenomena (Koskinen et al., 2011). Recently, the Helsinki UrBAN (Urban Boundary-layer Atmosphere Network, http://urban.fmi.fi) project has started a long-term intensive observational network to study physical processes in the atmosphere above the city (Wood et al., 2013). The network's key purpose is the understanding of the physical processes in the urban boundary layer such as fluxes of heat, momentum and exchanges of water vapor. Within this research framework, three dual-polarization C-band weather radars operate in the Helsinki metropolitan area. Fig. 1 shows the weather radars locations and the urban area of Helsinki. The Vantaa weather radar (hereafter VAN) is operated by the FMI, and it has been installed on the old water tower of Vantaa's Kaivoksela, close to the city's international airport (Saltikoff and Nevvonen, 2011). The Kumpula radar (KUM) is operated by the Department of Physics of the University of Helsinki (UHEL), and it is located on the roof of the main building of the Kumpula campus, about 4 km northeast from the city center. The Kerava radar (KER) is located northward about 23 km from the city center, operated by Vaisala Oyj, and it is operated by the UHEL radar meteorology group for research purposes. Given the antenna resolution and the relatively short distances between the radar sites, these instruments can provide rainfall estimations for the city of Helsinki with the satisfactory spatial resolution required hydrological and hydraulic models. The antenna pointing accuracy for the three weather radars is about 0.1°, and their lowest elevations of the operational scans are 0.4 and 0.7° elevation for VAN and KER, respectively, and 0.5 and 1.0° elevation for KUM. Table 1 summarizes the weather radar locations and their main characteristics.

Methodology

ALS data consist of geo-located points (about 7–5 million per tile), reporting the surface height. Fig. 2 shows ALS tiles used in this analysis. These points have to be projected from their native map projection to radar-centric coordinate system, i.e., azimuth from north and slant range from the antenna. ALS points lower than the antenna pedestal have been discharged as negative elevations are not used by the three Helsinki radars. ALS data have been visually inspected to remove isolated and suspicious points; then, the obstacle profile has been derived as a staircase function. When the beam intercepts an obstacle, beam occultation then occurs. Using beam "atmospheric standard propagation" equations, it is possible to derive the height of the beam with respect to the Earth's surface, given antenna elevation and azimuth. Recalling Doviak and Zrnić (1984), the height of the center of the beam h, leaving the radar with elevation θ_e, is given by the well-known equation

$$h = k_e \left[\frac{\cos\theta_e}{\cos\left(\theta + s/k_e a\right)} \right], \tag{1}$$

while the following two equations relate to r and θ_e:

$$h = \left[r^2 + (k_e a)^2 + 2 r k_e a \sin\theta \right]^{1/2} - k_e a, \tag{2}$$

$$s = k_e a \sin^{-1}\left(\frac{r\cos\theta_e}{k_e a + h} \right), \tag{3}$$

where r is the great circle distance from the antenna and s the slant range; k_e depends on the refractivity gradient, which is a function of atmospheric temperature, humidity and pressure. Observations demonstrate that the refractive index gradient in the first one or two kilometers of the atmosphere is often constant, so the effective radius $k_e a$ is approximately $\frac{4}{3}a$: these conditions are usually referred to as "standard propagation conditions". Inverting Eqs. (1), (2) and (3), it is also possible to obtain the ground range (great circle distance), the height above the Earth's surface given the slant range (along the beam) and the elevation angle. Given a surface profile in the field of view of the radar and the antenna radiation pattern, the fraction of blocked beam has to be derived to estimate the beam occultation. Although the antenna radiation pattern is usually complex, assuming a symmetrical antenna with all energy focused in the main lobe, it is a common approximation to calculate the integral of the total emitted power. Considering a two-dimensional Gaussian illumination function, the antenna radiation pattern is given by

$$f(\phi) = \exp\left[-\ln(2) \left(\frac{\phi}{\phi_{3\,\mathrm{dB}}} \right)^2 \right], \tag{4}$$

where $\phi_{3\,\mathrm{dB}}$ is the angular separation in which the magnitude of the radiation pattern decreases by 50 % (or −3 dB), and it is named half-power beamwidth. The angle ϕ is measured from the point of maximum radiation. The effective beamwidth for the azimuth scanning antenna can be derived according to Doviak and Zrnić (1984) (Sect. 7.8). For the Helsinki weather radars the lowest plan position indicator (PPI) scan rate is $15^\circ\,\mathrm{s}^{-1}$, the pulse repetition frequency (PRF) is 1000 Hz and 32 samples are averaged. The

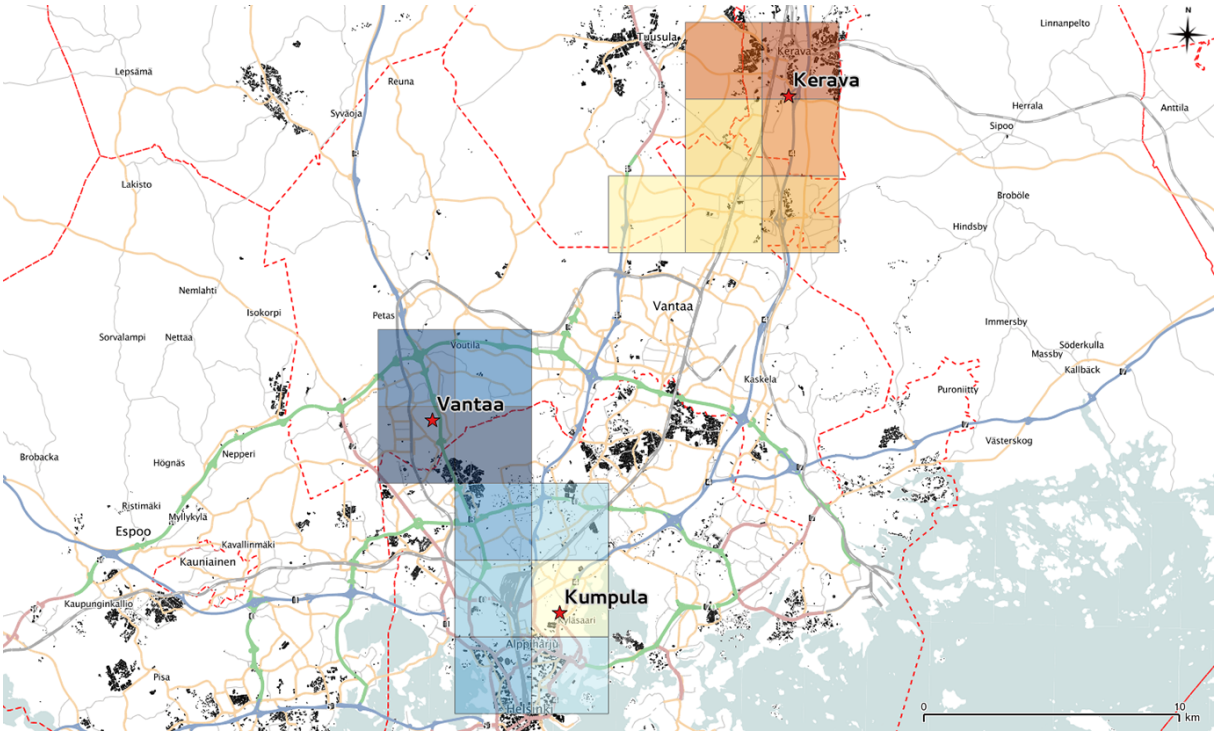

Figure 2. The ALS data tiles considered in this study.

beam propagation has been modeled, dividing the antenna beam in rays of varying azimuth and elevation in the range of 3 dB width and applying Eqs. (1), (2) and (3): the emitted power for each ray is given by $f(\phi)$ multiplied by P_0 (the emitted power in the center of the beam). When the obtained ray height is lower than the ALS point height, the ray is considered blocked. The total expected blocking is derived as the ratio between weighted emitted power blocked and unblocked rays. Considering that the antenna positioning accuracy for the Helsinki weather network is 0.1°, several antenna positions have been randomly generated from a uniform distribution, varying in both azimuth and elevation in a range of -0.1 to $+0.1°$. In this way, it is possible to evaluate more robustly the expected PBB and its uncertainty taking into account the antenna positioning accuracy. After having obtained the PBB estimations, the results are checked by locating the obstacles by the GIS interface QGIS (2015), by web mapping (AAVA open data, Google Maps and OpenStreetMap) and by evaluating their pictures. This methodology cannot be applied to obstacles located within antenna near-field region. For larger antennas the boundary between the near-field and far-field region can be roughly calculated as $R = \frac{2D^2}{\lambda}$, where D is the antenna diameter and λ is the wavelength. Substituting antenna diameter and wavelength for Helsinki radars ($D = 4.2$ m and $\lambda = 0.0533$ m), the far-field region starts at about 662 m from the antenna center.

3 Results

The described processing has been implemented for KUM, VAN and KER radars to estimate at lowest elevations the partial beam blockages caused by buildings, trees or masts. Hereafter, overall results are reported and specific cases are analyzed for each weather radar of the Helsinki network.

3.1 Kumpula weather radar

Located on the roof of the University of Helsinki building on the Kumpulan campus, the KUM radar is the closest to the city center (only about 4 km). Fig. 3 shows the 360° panoramic view from the antenna tower of Kumpula radar. The main obstacles are visible from the picture: Paavalin Kirkko bell tower 800 m from the antenna at 192° azimuth, the two tall residential buildings in Itä-Pasila (252°) and YLE Studiotalo buildings with their television tower (Pasilan TV-masto) at about 270°.

Kumpula radar lowest elevations of the operational scan are 0.5 and 1.0°. Considering the elevation at 0.5°, several strong partial beam blockages occur. The strongest expected PBBs take place at 252 and 253° due to Itä-Pasila residential buildings, and the television tower at 271°. At 169 to 170° azimuth the huge Hanasaari power plant, about 2.0 km from the radar, causes a partial beam blockage by two power plan chimneys: one 150 m tall with 8 m diameter, the other 100 m tall with 6 m diameter. At 170° azimuth, the chimneys cause 3.8 dB two-way losses (median value) with a 1.4 dB inter-

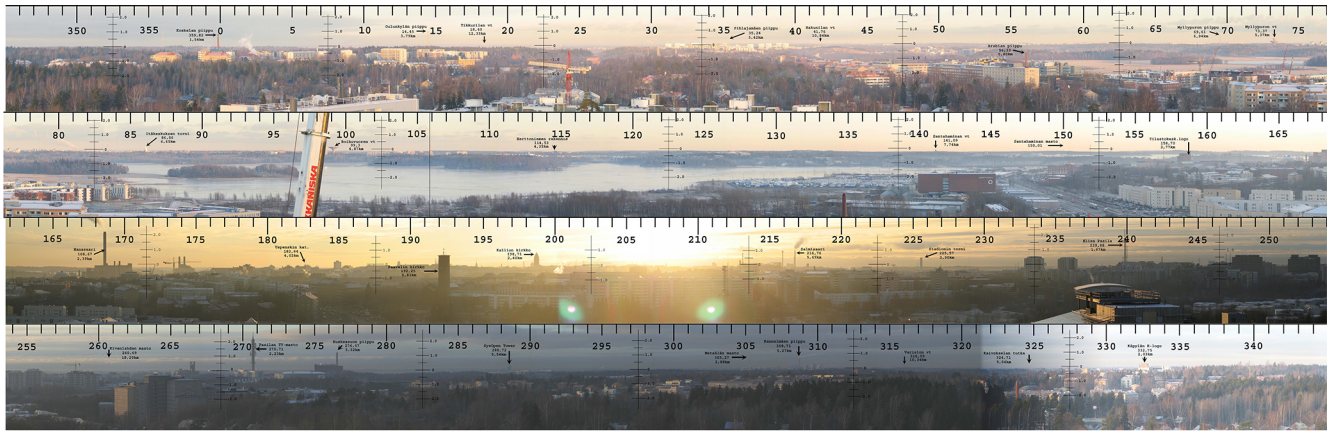

Figure 3. The 360° panoramic view from the antenna tower of Kumpula radar.

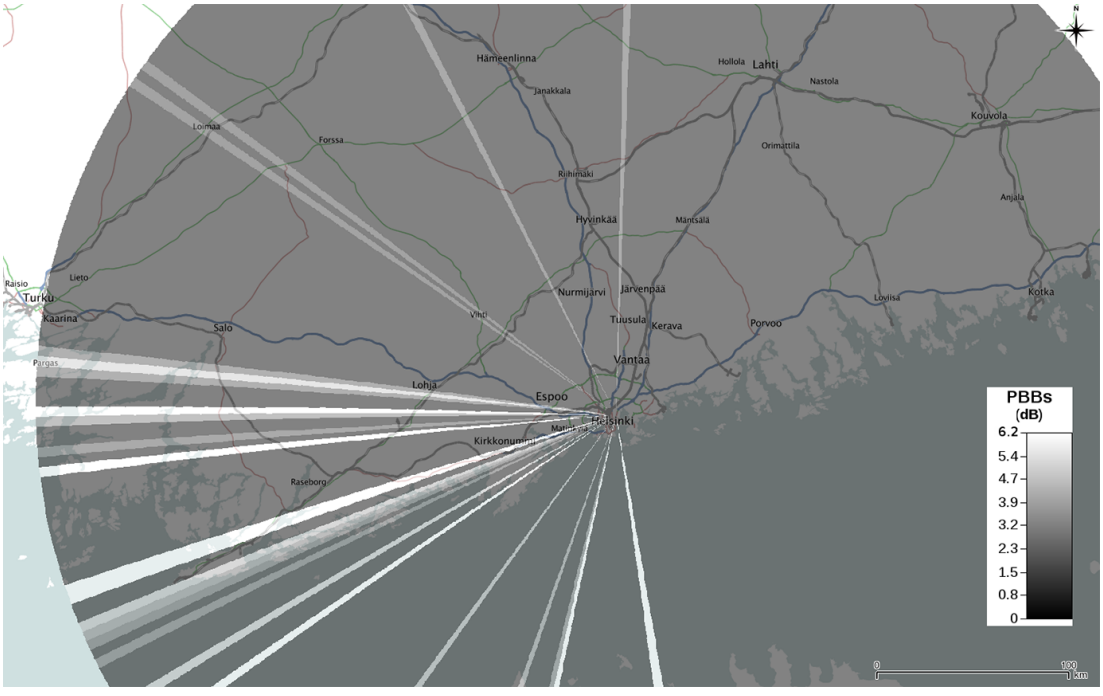

Figure 4. Estimated partial beam blockages for Kumpula radar.

quantile range: this uncertainty estimation is derived by randomly sampling 100 azimuths and elevations within a range between −0.1 and 0.1°. The other relevant PPBs happen at 192° azimuth (4.4 dB), corresponding to Paavalin Kirkko bell tower, 0.8 km from the antenna, and between 233 and 245°. Finally, the Linnanmäki amusement park of Helsinki at 216° azimuth causes 2.3 dB two-way losses; tall residential buildings in Itä-Pasila at 236° (4.5 dB) and some minor PBBs happen between 304 and 347°: they are caused by a mast and forest canopy in the Central Park of Helsinki and by residential buildings in Käpylä. Fig. 4 summarizes the estimated PBBs for Kumpula weather radar.

Hereafter, as an explanatory example, we focus on the occultation caused by the Paavalin Kirkko bell tower. The left side of Fig. 5 shows the Kumpula radar location and the bell tower located at about 0.8 km to the south. The superimposed points are ALS data. The expected partial beam blocking, derived for 0.5° elevation, is also shown in Fig. 5. The color shading represents the beam power distribution within 3 dB beamwidth, relative to the maximum in the center. The dark blue color shows the occultation caused by the bell tower; its shape is derived from the ALS points: ALS data have been reprojected in radar-based coordinates (azimuth and elevation), and the mask is derived as a staircase function. The two-way estimated beam blockage by 100 samples around

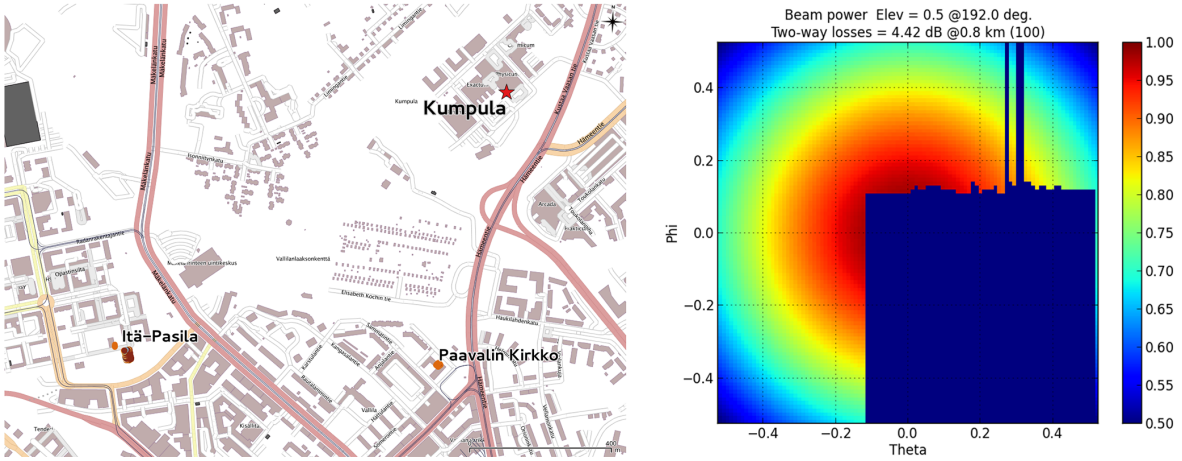

Figure 5. Left: the Kumpula radar and the bell tower map, Helsinki. Right: estimated radar beam blocking at 0.7° elevation and 192° azimuth. Color represents the beam power normalized to one in the beam center.

192° azimuth and 0.5° elevation is 4.4 dB (median value), and the inter-quantile range is 0.9 dB.

As expected, when the antenna is raised up to 1.0° elevation, the radar visibility greatly improves: some PBBs disappear, others reduce to less than 1 dB and the strongest ones sensibly decrease. The Paavalin Kirkko partial beam blockage reduces to less than 1 dB, Itä-Pasila residential area PBB reaches 1.5 dB and YLE Studiotalo decreases to 5.0 dB. All PBBs for azimuths greater than 275° range disappear. Table 2 summarizes the estimated partial beam blockages, deduced by ALS data analysis, for Kumpula radar, reporting the location of the blockage, the type, the azimuth and the distance from the weather radar; then two-way losses estimated by varying azimuth and elevation (median and inter-quantile values are reported) for the lowest operational PPI scans at 0.5 and 1.0°.

3.2 Vantaa weather radar

The radar (84 m a.s.l., above sea level) is located over the Kaivoksela water tower, in Kaivoksela, Vantaa, about 8 km from Helsinki International Airport to the southwest. Even at the lowest elevation (0.4°), the radar visibility is pretty good, except for minor PBBs between 212 and 214° (about 1 dB) azimuths, corresponding to Malminkartano hill, 90 m a.s.l. altitude. The main obstacle is the huge Myyrmäki water tower, a concrete tower 47 m tall and 41 m in diameter with a capacity of 4500 m^3. The tower is located at about 2 km at 272° azimuth (Fig. 6). Repeating the above-mentioned process – that is, randomly varying the azimuth and elevation 100 times within the antenna positioning uncertainty – the median value of two-way losses is 7.2 dB with a 2.5 dB inter-quantile range. When the elevation is raised up to 0.7°, the beam occultation decreases to 2.1 dB with a 0.9 dB inter-quantile range. The beam is completely free only at 1.0° elevation. Another relevant partial beam blockage (2.7 dB with 1.1 inter-quantile range) occurs at 309° with 0.4°, corresponding to the Martinlaakson power plant, 2.3 km from the Vantaa radar: the main things responsible for this beam occultation are its four 60 m tall chimneys. When the antenna elevation is raised to 0.7° elevation, the partial beam blockage reduces to 0.9 ± 0.2 dB.

3.3 Kerava weather radar

The Kerava weather radar, a Vaisala WRM200, is located on the top of a water tower in the town of Kerava at 95 m a.s.l. At 0.4° elevation only two partial beam blockages (about 1.2 dB) occur at 356° azimuth, corresponding to an industrial plant 2.4 km from the radar, and at 106° azimuth, corresponding to a mast located 0.9 km from the radar site. Raising the antenna to 0.7° elevation, all PBBs disappear.

4 Discussion

The evaluation of PBBs using airborne laser scan data in the metropolitan area of Helsinki showed that severe beam occultations occur for low elevations. This result could not be obtained from digital terrain models as they do not include trees, buildings and constructions. As shown by the PPB analysis, Kumpula is the weather radar in Helsinki most effected by occultations caused by metropolitan buildings and constructions: for this reason hereafter we focus on this radar.

In order to verify the PBBs derived from ALS data, stratiform precipitation events that hit the Helsinki area for several hours have been considered. On 22 September 2014, a warm front associated with a low centered over Poland moved east, causing extended rainfall over southern Finland. On the same day at 12:00 UTC, the radiosounding in Jokioinen (WMO code 02963) recorded the freezing level at about 1900 m a.s.l. As mentioned, in the low troposphere, the beam propagation depends on the variation of the refractive index n, for

Table 2. Kumpula weather radar partial beam blockages estimated from ALS data.

Location	Type	Azimuth	Distance (km)	Two-way losses (dB) 0.5°	1.0°
Korskela Forsby	Chimney	0°	1.5	1.3 ± 0.1	Free
Hanasaari	Power plan chimneys	169°	2.0	3.8 ± 1.4	< 1.0
Hanasaari	Power plan chimneys	170°	2.0	3.7 ± 0.2	< 1.0
Paavalin Kirkko	Bell tower	192°	0.8	4.4 ± 0.9	< 1.0
Paavalin Kirkko	Bell tower	193°	0.8	1.6 ± 0.7	< 1.0
Kallion Kirkko	Bell tower	199°	2.4	1.9 ± 0.1	Free
Linnanmäki	Amusement park	216°	2.2	2.3 ± 0.2	Free
Itä-Pasila	Residential area	236°	1.3	4.5 ± 0.1	Free
Itä-Pasila	Residential area and mast	240°	1.7	2.7 ± 0.3	1.5 ± 0.3
Itä-Pasila	Residential area	245°	1.6	1.3 ± 0.1	Free
Itä-Pasila	Residential area and two masts	247°	1.6	1.2 ± 0.1	Free
Itä-Pasila	Residential area and two masts	248°	1.7	1.8 ± 0.2	Free
Itä-Pasila	Residential area and two masts	249°	1.7	2.6 ± 0.2	Free
Itä-Pasila	Residential area	252°	1.4	5.6 ± 0.1	Free
Itä-Pasila	Residential area	253°	1.4	6.0 ± 0.6	Free
YLE Studiotalo	Industrial buildings	265°	2.4	3.9 ± 0.5	Free
YLE Studiotalo	Industrial buildings	267°	2.4	1.2 ± 0.5	Free
YLE Studiotalo	Television tower	270°	2.2	1.9 ± 0.6	Free
YLE Studiotalo	Television tower	271°	2.2	6.2 ± 0.6	5.0 ± 0.4
Ilmala	Industrial buildings	275°	2.6	1.4 ± 0.3	Free
Ilmala	Industrial buildings	276°	2.6	3.0 ± 0.1	Free
Ilmala	Industrial buildings	277°	2.6	1.4 ± 0.3	Free
Central Park	Trees and mast	305°	3.1	1.0 ± 0.2	Free
Central Park	Trees	307°	3.0	1.0 ± 0.2	Free
Käpylä	Residential area and trees	333°	1.8	1.2 ± 0.2	Free

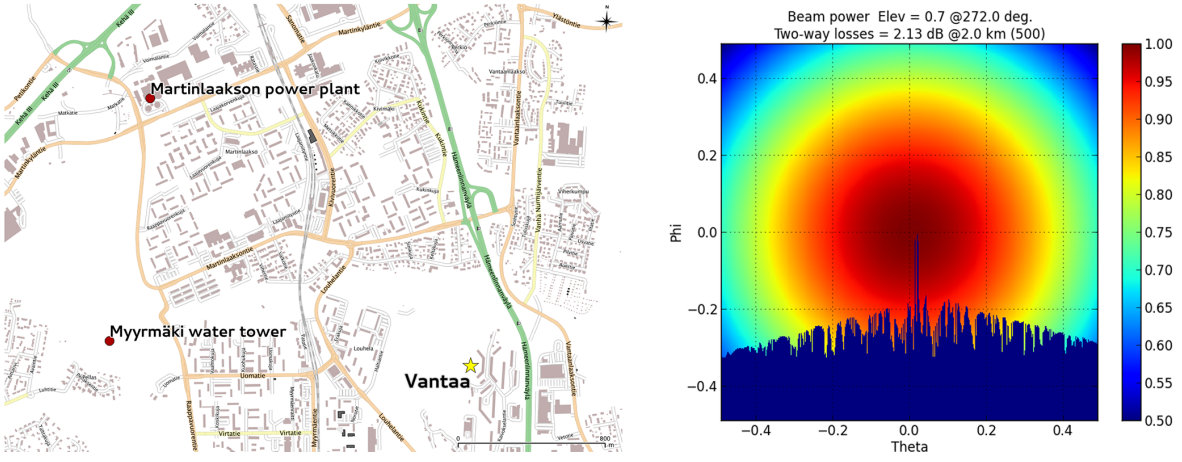

Figure 6. Left: Vantaa radar and Myyrmäki water tower. Right: estimated radar beam blocking at 0.7° elevation and 272° azimuth. Color represents the beam power normalized to one in the beam center.

dimensional reasons usually expressed in terms of refractivity $N = (n-1) \times 10^6$. For microwaves, this parameter can be estimated according to Bean and Dutton (1968):

$$N = \frac{77.6}{T} \times \left(P + 4810\frac{e}{T}\right), \quad (5)$$

where T is the dry-air temperature in degrees Kelvin; P is the atmospheric pressure in mbar or hPa; and e is the water vapor pressure, also expressed in mbar or hPa. The typical values of the refractivity vertical gradient $-\frac{\partial N}{\partial z}$ are around $-40\,\mathrm{km}^{-1}$. Under favorable conditions for anomaly propagation, the refractivity gradient reaches values equal to or lower than $-157\,\mathrm{km}^{-1}$. Applying Eq. (5) to Jokioinen ra-

Table 3. Kumpula weather radar two-way losses at 0.5° elevation: comparison of estimated values from ALS data and observed ones derived by 24 h accumulation rainfall. Italic-font rows report anomalies that are discussed in the text.

Location	Type	Azimuth	Distance (km)	Two-way losses at 0.5° (dB) Estimated	Observed
Korskela Forsby	Chimney	0°	1.5	1.5	2.2
Hanasaari	*Power plan chimneys*	*169°*	*2.0*	*3.8*	*1.8*
Hanasaari	*Power plan chimneys*	*170°*	*2.0*	*3.7*	*1.8*
Paavalin Kirkko	Bell tower	192°	0.8	4.4	3.2
Paavalin Kirkko	Bell tower	193°	0.8	1.6	1.8
Linnanmäki	Amusement park	216°	2.1	2.3	1.8
Itä-Pasila	Residential area	236°	1.3	4.5	5.5
Itä-Pasila	Residential area and mast	240°	1.7	2.7	2.6
Itä-Pasila	Residential area	245°	1.6	1.3	2.9
Itä-Pasila	*Residential area and two masts*	*247°*	*1.6*	*1.2*	*9.1*
Itä-Pasila	*Residential area and two masts*	*248°*	*1.6*	*1.8*	*9.1*
Itä-Pasila	*Residential area and two masts*	*249°*	*1.7*	*2.6*	*9.1*
Itä-Pasila	Residential area	252°	1.4	2.6	8.7
Itä-Pasila	Residential area	253°	1.4	5.6	4.5
YLE Studiotalo	Industrial buildings	265°	2.4	3.9	2.4
YLE Studiotalo	Industrial buildings	267°	2.4	1.2	1.7
YLE Studiotalo	Television tower	270°	2.2	1.9	1.8
YLE Studiotalo	Television tower	271°	2.2	6.2	4.1
Ilmala	Industrial buildings	275°	2.6	1.4	3.1
Ilmala	Industrial buildings	276°	2.6	3.0	4.3
Käpylä	Residential area and trees	333°	1.8	1.2	1.4

diosounding data, it is possible verify that on 22 September 2014 there were standard atmosphere propagation conditions ($-\frac{\partial N}{\partial z} \sim -30\,\mathrm{km}^{-1}$) in the lowest 3 km.

Fig. 7 reports the total rainfall accumulation from 00:00 to 24:00 UTC on 22 September 2014 derived by the Kumpula radar 0.5° elevation horizontal reflectivity PPI. The heaviest precipitation occurred to the west and northwest of Helsinki. Along the line passing the radar site from northwest to southeast, the "zero-isodop" is visible due to Doppler filtering of near-zero Doppler velocity data (Saltikoff, 2012). Meanwhile, several partial beam blockages are evident; close to the radar the artificial enhancement of the precipitation accumulation caused by residual clutter is also clearly visible. The total rainfall accumulation has been derived from PPI horizontal reflectivity by applying the well-known relationship Z–R (Marshall and Palmer, 1948):

$$Z = aR^b, \tag{6}$$

where Z is the radar reflectivity in linear units, R is the rainfall rate in mm h^{-1}, and a and b are two empirical coefficients that here are assumed $a = 300$ and $b = 1.5$. Considering the ratio between unblocked and blocked reflectivity and applying logarithm to Eq. (6), the two-way losses can be derived from the following equation:

$$L_{\mathrm{dB}} = \frac{\mathrm{dB}\,Z_{\mathrm{blocked}}}{\mathrm{dB}\,Z_{\mathrm{total}}} = b \times 10\log_{10}\frac{R_{\mathrm{blocked}}}{R_{\mathrm{total}}}, \tag{7}$$

where L_{dB} is the total observed estimation, Z_{blocked} and $Z_{\mathrm{unblocked}}$ are now expressed in units of dB, and where R_{blocked} and $R_{\mathrm{unblocked}}$ are evaluated behind and beyond the obstacle. To determine the ratio $R_{\mathrm{blocked}}/R_{\mathrm{unblocked}}$, several profiles of the rainfall accumulation across the partial beam blockage have been manually selected, using the QGIS interface. The strong constraint is manually identifying profiles within regions of a relatively uniform rainfall field. Fig. 8 shows an example of a rain profile selected to estimate the partial beam blockages between 270 and 271°; the x axis reports the distance in meters from the northeast point to the southwest one along the profile. By applying statistical error propagation rules to the Eq. (7), it is possible to evaluate uncertainties in observed occultation retrieval. Assuming the unblocked average rainfall field to be about 8 mm and blocked rainfall observation to be about 3 mm, both with 1 mm uncertainty, an error of 1.4 dB is obtained.

Table 3 reports the comparison between PBB two-way losses estimated by ALS data and observed values derived from total rainfall accumulation. Although it has been considered a relatively short-time rainfall accumulation, the good agreement between expected and retrieved values is evident. There are two exceptions: at 170° azimuth (Hanasaari power plant), and between 247 and 249° azimuths (Itä-Pasila residential area). In the first occultation there is an overestimation of the beam blockage, which can be explained by a rough reconstruction of the power plant using ALS data.

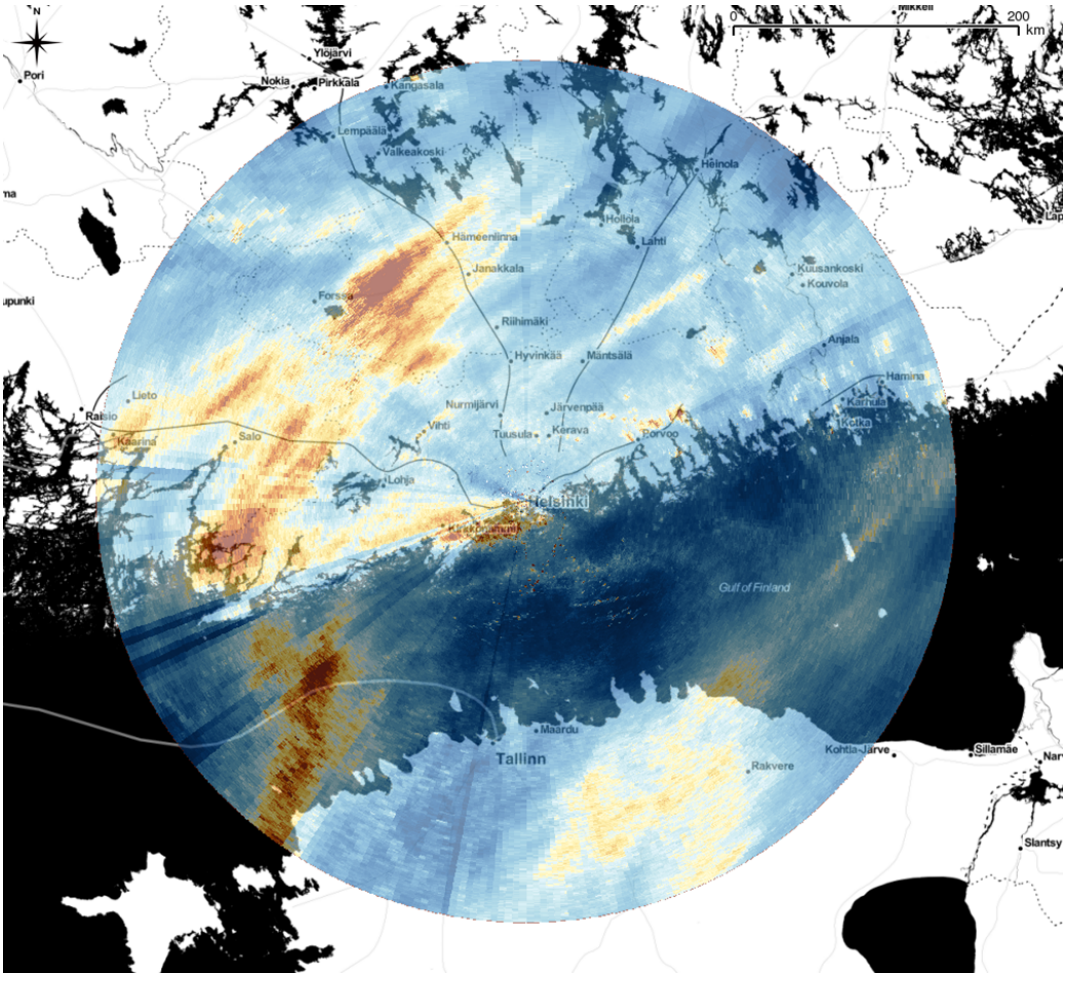

Figure 7. 24 h rainfall accumulation on 22 September 2014 from Kumpula PPI reflectivity at 0.5° elevation.

This unsophisticated reconstruction in the case of complex constructions can contribute to PBB underestimations.

Two 20 m tall mobile masts, located above the roof of a building in Itä-Pasila, were partially detected by the airborne laser scanning survey in 2008: they are responsible for the large underestimation of the partial beam blockage in Itä-Pasila. The right side of Fig. 9 shows the radar beam center, ALS data and Itä-Pasila buildings. Firstly, the beam is partially occulted by the Eläketurvakeskus building; then after passing close to a flagpole, the beam center hits the mobile mast 1: Fig. 9 also shows a picture of the two masts in Itä-Pasila from Google Street View. However, the architectural complexity of buildings in Itä-Pasila and the their rough reconstruction using ALS data can also contribute to the overall underestimation. Excluding these two cases, the agreement between estimated and observed partial beam blockages is generally good. The normalized mean bias is 7 % and the root mean square error is 1.4 dB as shown in Fig. 10. While the aforementioned analysis of Kumpula radar occultation has demonstrated the validity of this methodology, this study makes evident some limitations that can affect the two-way-loss estimation accuracy. Airborne laser scanning campaigns are expensive and take place rarely: in the case of Helsinki, ALS data were collected in 2008. Recent buildings and urbanization changes can remove or introduce new beam occultations that cannot be estimated. Two cases related to Kumpula radar can explain quite well how the urban development affects PBB estimations. From the daily rainfall accumulation (Fig. 5), a beam blocking is clearly visible at 62° azimuth in the direction of the city Porvoo. The observed two-way losses are about 2.6 dB, but this occultation is not detected by ALS data: recent tall buildings and cranes in the Arabia district, Helsinki, 900 m from the Kumpula radar are responsible for this occultation. The opposite instance happens to the north: the Korskela Forsby chimney causes a partial beam blockage at 0° azimuth, both estimated from ALS data and evident in 24 h rainfall accumulation on 22 September 2014 (Fig. 5). However, this industrial plant has since been demolished: this partial beam blockage never occurs in recent observations.

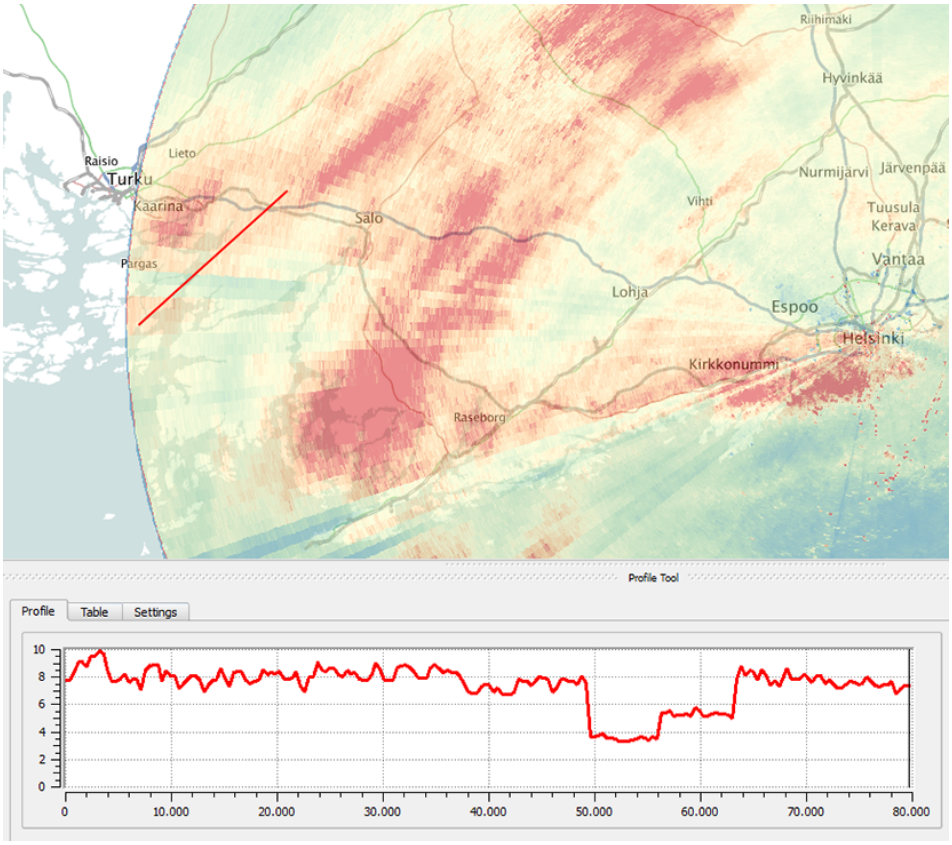

Figure 8. Example of rain profile (mm) on 22 September 2014 along the red line used to estimate the partial beam blockage for the Kumpula weather radar. The x axis reports distance in meters from northeast to southwest.

Figure 9. Left: Itä-Pasila partial beam blockage. Lines show beam center path for 252, 248 and 240° azimuths; dots are ALS data, and colors correspond to altitude above sea level (brown: 60 m; yellow: 65 m; orange: 70 m; red 75 m; and purple: $>$ 75 m). The two masts and a flagpole along the beam path are also reported. Right: Google Street View of the two masts from Böle bro (Itä-Pasila, Helsinki. Map. Google Street View. Google, June 2009. Web. 3 February 2016).

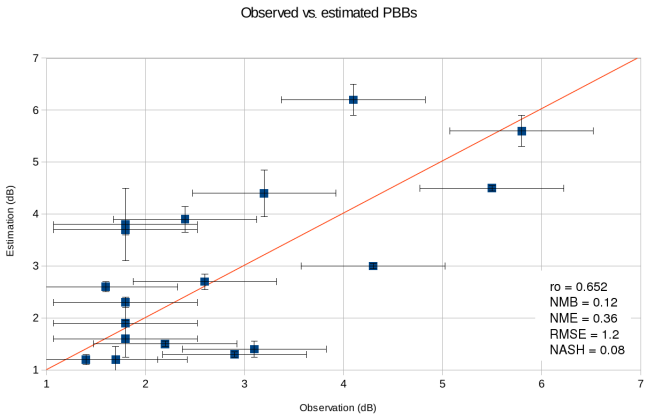

Figure 10. The scatterplot between laser-scanning-based estimated two-way losses and observed ones for Kumpula radar with 0.5° elevation. Ro is the Pearson correlation coefficient, NMB the normalized mean bias, NME the normalized mean error, RMSE the root mean square error and NASH the Nash–Sutcliffe model efficiency coefficient.

The shape of obstacles has been gathered using a simple step function model: this approximation leads to underestimations or overestimations in the case of masts or complexly shaped buildings. The estimated uncertainty has been derived considering the nominal antenna pointing accuracy (0.1°) under the assumption of standard atmospheric propagation: including antenna control in elevation, temperature variations and different atmospheric propagation or even duct conditions, this uncertainty is expected to increase. Finally, the manual selection of rainfall profiles across the beam occultation could lead to some uncertainties. In a future work, an objective selection of these profile could be implemented on the basis of directional constraints in rainfall spatial variability, evaluating the rainfall semi-variogram or the ratio of the standard deviation to the arithmetic mean depth.

5 Conclusions

Urban hydrology requires rainfall observations with high resolution in space and time that weather radars can timely provide when located close to the urban areas. However, the need to use low antenna elevations for quantitative precipitation estimations to get the weather radar observations close to the ground is in contrast with widespread beam occultations caused by buildings, trees and constructions. In an urban environment the weather radar visibility derived from digital elevation models, even with very high spatial resolution, underestimates partial beam blockages (Zhang et al., 2013). The increased availability of airborne laser scan data over metropolitan areas can overcome this limitation. Analyzing Helsinki weather radars, this study demonstrates that accurate ALS data and GIS functionality can locate azimuthal angles where partial beam blockages occur, estimating quantitatively the associated two-way losses. With an appropriate beam propagation model and a simple reconstruction of buildings and forest canopy, it is possible to estimate quantitatively beam occultations, including the uncertainties related to antenna pointing accuracy. The comparison between estimated and observed PBBs, derived from 24 h stratiform rainfall accumulation, has demonstrated a good agreement both qualitatively, in the identification of affected azimuths, and quantitatively, in two-way-loss estimations. Nevertheless, this analysis has also shown some limitations of the methodology due to urban developments and/or to the rough reconstruction of the obstacles. First of all, up-to-date ALS data are needed. The case of the Korskela Forsby chimney is a classic example: the expected beam blockage derived from the ALS campaign in 2008 is not in agreement with recent weather radar observations due to the obstacle demolition. However, as the economic and processing limitations of laser scan data decrease, data coverage and data availability increase. Moreover, in urban landscapes, campaign cost reduction and representativeness improvement can be achieved by the synergical use of airborne, mobile and terrestrial laser scans (Turner, 2013). Metal mobile masts are particularly difficult to reconstruct from ALS data: to partially overcome this limit, the use of more complex algorithms (Vosselman et al., 2001; Dorninger et al., 2008 or Kada and McKinley, 2009) for a more accurate reconstruction of the obstacles could reduce the spread between estimated and observed two-way losses. Blockage calculations for rural radars using ALS data have an additional limit: at midlatitudes the blockage by deciduous trees is seasonal, making ALS results different from summer to winter. Finally, an additional source of uncertainty is actual atmospheric refractivity conditions as beam standard atmospheric propagation conditions have been assumed. However, partial beam-blocking estimations from ALS data can be used to redefine the scan strategy of weather radars located in urban areas, optimizing the lowest elevation angles with respect to the obstacles close to the antenna. Provided an accurate 3-D building reconstruction, airborne laser scanning data could be used to model the expected ground clutter return from the metropolitan area. Finally, by simulating 3-D obstacles, this methodology can be used to evaluate the impact of new buildings, infrastructure or changes in the urban areas close to the antenna on weather radar measurements.

6 Data availability

The radar data used in this study are available by request from D. Moisseev (dmitri.moisseev@helsinki.fi). The laser scanning data are available from http://www.maanmittauslaitos.fi/en/professionals/web-services/open-data-file-download-service (NLS, 2016).

Acknowledgements. This study has been supported by the Academy of Finland (grants 263333 and 305175) and the Academy of Finland Centre of Excellence (grant 272041). The authors would like to thank Matti Leskinen and Niko Tollman for the panoramic photo of the Helsinki skyline used in this paper.

Edited by: G. Vulpiani
Reviewed by: four anonymous referees

References

Ackermann, F.: Airborne laser scanning–present status and future expectations, ISPRS J. Photogramm., 54, 64–67, doi:10.1016/S0924-2716(99)00009-X, 1999.

Ahokas, E. and Kaartinen, H.: On the quality checking of the airbone laser scanning-based nation wide elevation model in Finland, available at: http://www.isprs.org/proceedings/xxxvii/congress/1_pdf/44.pdf (last access: 12 July 2014), 2013.

Bean, B. R. and Dutton, E. J.: Radio Meteorology, Dover Publications, 435 pp., 1968.

Bech, J., Codina, B., Lorente, J., and Bebbington, D.: The sensitivity of single polarization weather radar beam blockage correction to variability in the vertical refractivity gradient, J. Atmos. Ocean. Tech., 20, 845–855, doi:10.1175/1520-0426(2003)020<0845:TSOSPW>2.0.CO;2, 2003.

Berne, A., Delrieu, G., Creutin, J., and Obed, C.: Temporal and spatial resolution of rainfall measurements required for urban hydrology, J. Hydrol., 299, 166–179, 2004.

Dorninger, P. and Pfeifer, N.: A comprehensive automated 3D approach for building extraction, reconstruction, and regularization from airborne laser scanning point clouds, Sensors, 8, 7323–7343, 2008.

Doviak, R. J. and Zrnić, D. S.: Doppler radar and weather observations, Dover Publication, Inc., Mineola, New York, ISBN-10: 0-486-45060-0, 1984.

Einfalt, T., Arnbjerg-Nielsen, K., Golz, C., Jensen, N.-E., Quirmbach, M., Vaes, G., and Vieux, B.: Towards a roadmap for use of radar rainfall data in urban drainage, J. Hydrol., 299, 186–202, 2004.

Fornasiero, A., Alberoni, P. P., and Bech, J.: Statistical analysis and modelling of weather radar beam propagation conditions in the Po Valley (Italy), Nat. Hazards Earth Syst. Sci., 6, 303–314, doi:10.5194/nhess-6-303-2006, 2006.

Fulton, R. A., Breidenbach, J. P., Seo, D., Miller, D., and O'Bannon, T.: The WSR-88D Rainfall Algorithm, Weather Forecast., 13, 377–395, 1998.

Giangrande, S. E. and Ryzhkov, A. V.: Calibration of dualpolarization radar in the presence of partial beam blockage, J. Atmos. Ocean. Tech., 22, 1156–1166, 2005.

Guha-Sapir, D., Below, R., and Hoyois, P.: EM-DAT: The CRED/OFDA International Disaster Database, available at: www.emdat.be (last access: 2 December 2016), Université Catholique de Louvain, Brussels, Belgium, 2016.

Kada, M. and McKinley, L.: 3D building reconstruction from lidar based on a cell decomposition approach, International Archives of Photogrammetry, Remote Sensing and Spatial Information Sciences, 38, 47–52, 2009.

Kitchen, M., Brown, R., and Davies, A. G.: Real-time correction of weather radar data for the effects of bright band, range and orographic growth in widespread precipitation, Q. J. Roy. Meteorol. Soc., 120, 1231–1254, 1994.

Koskinen, J. T., Poutiainen, J., Schultz, D. M., Joffre, S., Koistinen, J., Saltikoff, E., Gregow, E., Turtiainen, H., Dabberdt, W. F., Damski, J., Eresmaa, N., Göke, S., Hyvärinen, O., Järvi, L., Karppinen, A., Kotro, J., Kuitunen, T., Kukkonen, J., Kulmala, M., Moisseev, D., Nurmi, P., Pohjola, H., Pylkkö, P., Vesala, T., and Viisanen, Y.: The helsinki testbed: A mesoscale measurement, research, and service platform, B. Am. Meteorol. Soc., 92, 325–342, doi:10.1175/2010BAMS2878.1, 2011.

Krajewski, W. F., Ntelekos, A. A., and Goska, R.: A GIS-based methodology for the assessment of weather radar beam blockage in mountainous regions: Two examples from the US NEXRAD network, Comput. Geosci., 32, 283–302, doi:10.1016/j.cageo.2005.06.024, 2006.

Kucera, W. F. K., Paul, A., and Young, C. B.: Radar beam occultation studies using gis and dem technology: an example study of Guam, J. Atmos. Ocean. Tech., 21, 995–1006, 2004.

Lang, T. J., Nesbitt, S. W., and Carey, L. D.: On the Correction of Partial Beam Blockage in Polarimetric Radar Data, J. Atmos. Ocean. Tech., 26, 943–957, 2009.

Marshall, J. S. and Palmer, W. M.: The distribution of raindrops with size, J. Meteorol., 5, 165–166, 1948.

NLS: National Land Survey of Finland, Laser scanning data, available at: http://www.maanmittauslaitos.fi/en/digituotteet/laser-scanning-data last access: 19 January 2016.

QGIS: Development Team, QGIS Geographic Information System. Open Source Geospatial Foundation Project, available at: http://qgis.osgeo.org (last access: 2 October 2016), 2015.

Saltikoff, E.: Measuring Snow with Weather Radar, in: Doppler Radar Observations, edited by: Bech, J. and Chau, J. L., 6, 159–174, Intech, Rijeka, Croatia, ISBN-13: 978-953-51-0496-4, doi:10.5772/2036, 2012.

Saltikoff, E. and Nevvonen, L.: First experiences of the operational use of a dual-polarisation weather radar in Finland, Meteorol. Z., 20, 323–333, 2011.

Shan, J. and Sampath, A.: Building extraction from LiDAR point clouds based on clustering techniques, Boca Raton, FL, CRC Press, 423–446, 2008.

Ten Veldhuis, J. A. E., Ochoa-Rodriguez, S., Bruni, G., Gires, A., van Assel, J., Wang, L., Reinoso-Rodinel, R., Kroll, S., Schertzer, D., Onof, C., and Willems, P.: Weather radar for urban hydrological applications: lessons learnt and research needs identified from 4 pilot catchments in North-West Europe, International Symposium, Weather Radar and Hydrology, Washington DC, April 2014.

Turner, A. B., Colby, J. D., Csontos, R. M., and Batten, M.: Flood Modeling Using a Synthesis of Multi-Platform LiDAR Data, Water, 5, 1533–1560, doi:10.3390/w5041533, 2013.

United Nations: The World Urbanization Prospects: The 2014 Revision, The United Nations: New York, availabale at: https://esa.un.org/unpd/wup/, (last access: 11 February 2016), 2014.

United Nations International Office for Disaster Risk Reduction (UNISDR): Revealing Risk, Redefining Development. Global Assessment Report on Disaster Risk Reduction, Geneva, Switzerland: UNISDR, 2011.

Vosselman, G. and Dijkman, S.: 3D building model reconstruction from point clouds and ground plans, International Archives of Photogrammetry and Remote Sensing, 34, 37–43, 2001.

Wood, C. R., Järvi, L., Kouznetsov, R. D., Nordbo, A., Joffre, S., Drebs, A., Vihma, T., Hirsikko, A., Suomi, I., Fortelius, C., O'Connor, E., Moiseev, D., Haapanala, S., Moilanen, J., Kangas, M., Karppinen, A., Vesala, T., and Kukkonen, J.: An overview of the urban boundary layer atmosphere network in helsinki, B. Am. Meteorol. Soc., 94, 11, 1675–1690, doi:10.1175/BAMS-D-12-00146.1, 2013.

Zhang, P., Zrnić, D., and Ryzhkov, A.: Partial beam blockage correction using polarimetric radar measurements, J. Atmos. Ocean. Tech., 30, 861–872, doi:10.1175/JTECH-D-12-00075.1, 2013.